Infrared conductivity of hole accumulation and depletion layers in (Ga,Mn)As- and (Ga,Be)As-based electric field-effect devices

B. C. Chapler,[1] S. Mack,[2] L. Ju,[3] T. W. Elson,[1] B. W. Boudouris,[4] E. Namdas,[5] J. D. Yuen,[5] A. J. Heeger,[5] N. Samarth,[6]
M. Di Ventra,[1] R. A. Segalman,[4] D. D. Awschalom,[2] F. Wang,[3] and D. N. Basov[1]

[1]*Physics Department, University of California–San Diego, La Jolla, California 92093, USA*
[2]*Center for Spintronics and Quantum Computation, University of California–Santa Barbara, Santa Barbara, California 93106, USA*
[3]*Department of Physics, University of California at Berkeley, Berkeley, California 94720, USA*
[4]*Department of Chemical and Biomolecular Engineering, University of California at Berkeley, Berkeley, California 94720, USA*
[5]*Center for Polymers and Organic Solids, University of California–Santa Barbara, Santa Barbara, California 93106, USA*
[6]*Department of Physics, The Pennsylvania State University, University Park, Pennsylvania 16802, USA*

We have fabricated electric double-layer field-effect devices to electrostatically dope our active materials, either $x = 0.015$ $Ga_{1-x}Mn_xAs$ or $x = 3.2 \times 10^{-4}$ $Ga_{1-x}Be_xAs$. The devices are tailored for interrogation of electric field-induced changes to the frequency-dependent conductivity in the accumulation or depletion layers of the active material via infrared (IR) spectroscopy at room temperature. The spectra of the (Ga,Be)As-based device reveal electric field-induced changes to the IR conductivity consistent with an enhancement or reduction of the Drude response in the accumulation and depletion polarities, respectively. The spectroscopic features of this device are all indicative of metallic conduction within the GaAs host valence band (VB). For the (Ga,Mn)As-based device, the spectra show enhancement of the far-IR itinerant carrier response and broad mid-IR resonance upon hole accumulation, with a suppression of these features in the depletion polarity. These latter spectral features demonstrate that conduction in ferromagnetic (FM) $Ga_{1-x}Mn_xAs$ is distinct from genuine metallic behavior due to extended states in the host VB. Furthermore, these data support the notion that a Mn-induced impurity band plays a vital role in the electrodynamics of FM $Ga_{1-x}Mn_xAs$. We add that a sum-rule analysis of the spectra of our devices suggests that the Mn or Be doping does not lead to a substantial renormalization of the GaAs host VB.

I. INTRODUCTION

The electric field effect offers a decided advantage in investigations of electronic phenomena in complex materials. Namely, the charge density may be tuned without adding lattice disorder, and while keeping other sample properties intact. In this manner, electrostatic "doping" offers a "clean" approach to tune insulator-to-metal transitions (IMTs), as well as other phase transitions and electronic behavior.[1–5] In the vast majority of field-effect studies of complex materials, the experiments are limited to transport data. Experiments in the infrared (IR) regime, however, are uniquely suited to probe the evolution of electronic behavior in materials of interest as the charge density is electrostatically tuned. Infrared experiments serve as a contactless probe, sensitive to the narrow layer of charge accumulation or depletion formed at the interface between the active material and the gate insulator.[6] Moreover, experiments in the IR regime are desired because many characteristic energy scales in condensed matter systems fall within the IR range.[7,8]

In this work, we apply a gate-to-source voltage (V_{gs}) to produce an electric field effect in electric double-layer (EDL) devices. The electric field-induced changes to the frequency-dependent conductivity spectrum are probed by IR spectroscopy (see Fig. 1). The active material in our EDL devices is either $Ga_{1-x}Mn_xAs$, considered to be a prototypical ferromagnetic (FM) semiconductor, or a nonmagnetic p-doped counterpart system, $Ga_{1-x}Be_xAs$. Both Be and Mn act as single acceptors in a GaAs host, however Mn also adds a local magnetic moment. Therefore, $Ga_{1-x}Be_xAs$ serves as a useful

and less complicated material to contrast with the magnetic $Ga_{1-x}Mn_xAs$ system.

The advantages provided by field-effect studies are of extreme relevance to the physics of FM semiconductors in general, and of $Ga_{1-x}Mn_xAs$ in particular. The general agreement, and part of the technological appeal of $Ga_{1-x}Mn_xAs$, is that the ferromagnetism is mediated by itinerant holes.[9] This fact was established through more than a decade of systematic exploration of $Ga_{1-x}Mn_xAs$,[7,10–12] and it was validated through transport studies of the field effect in $Ga_{1-x}Mn_xAs$-based gated structures.[13–15] Thus all proposed mechanisms of ferromagnetism in $Ga_{1-x}Mn_xAs$ are intimately tied to the dynamics of the charge carriers.[11] However, even after a decade of research, the details of the electronic structure and magnetic interactions remain in dispute.[12,16,17] A central open issue has been, and remains, whether the mediating holes reside in a disordered valence band (VB)[10,18] or in an impurity band (IB), which can be detached from the host VB or otherwise retains the d character of the Mn dopants.[11,19–21]

II. BACKGROUND

Early after the initial growth of FM $Ga_{1-x}Mn_xAs$ films,[22] a p-d Zener exchange model was proposed to explain ferromagnetism.[18] In this model, hybridization of the impurity d wave functions with the p wave functions of the neighboring p elements results in a spin-split VB, which favors ferromagnetism provided that the Fermi level (E_F) resides within the VB. In contrast, initial measurements of the temperature
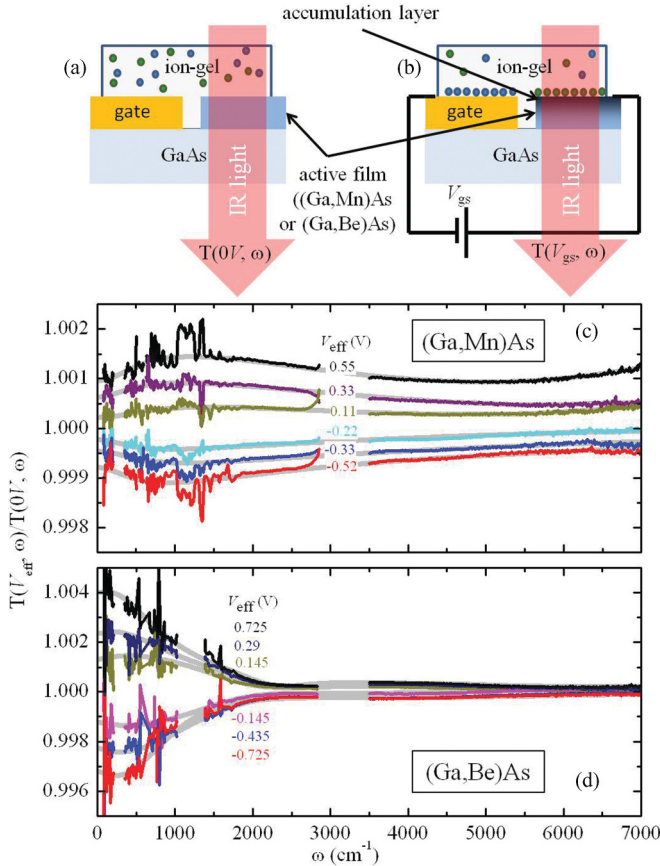
FIG. 1. (Color online) Panels (a) and (b) highlight the operating principle of the EDL field-effect devices used in our IR experiments, as described in the text. Panel (a) shows a device in the absence of any applied voltage, while panel (b) shows the device under applied V_{gs}. Panels (c) and (d) show the transmission spectra, under applied V_{gs}, through the $x = 0.015$ $Ga_{1-x}Mn_xAs$ and $x = 3.2 \times 10^{-4}$ $Ga_{1-x}Be_xAs$ based devices, normalized to their respective transmission spectrum at $V_{gs} = 0$. The data are cut near 300 cm^{-1} due to a GaAs phonon that eliminates transmission over the cut frequency range. The data are also cut where sharp features from strong vibrational modes in the ion gel obscure the spectra (near 1200 and 3200 cm^{-1}). Only select spectra are shown for clarity. The light gray lines in panels (c) and (d) are the model fits to the transmission spectra described in the text.

dependence of IR absorption spectra,[23] and then of the IR conductivity,[24] reported evidence of double-exchange-like interactions in FM $Ga_{1-x}Mn_xAs$. Later, detailed studies of the doping dependence of the IR conductivity at $T \ll T_c$ found strong evidence for E_F residing in an Mn-induced IB.[25] The key findings of this latter study came from sum-rule estimates of the carrier mass and the redshift of a broad mid-IR resonance in $Ga_{1-x}Mn_xAs$ with increasing hole concentration. These findings were seen as incompatible with E_F lying in a spin-split VB, invalidating the p-d Zener exchange model for $Ga_{1-x}Mn_xAs$. Theoretical calculations, however, showed that a mid-IR resonance can arise from intra-VB excitations,[26] and the screening of disorder could explain a redshift trend of the resonance.[27] Following this, IR experiments performed at room temperature found a blueshift trend as the hole concentration was increased.[28] Thus a monotonic trend in the

mid-IR resonance versus hole concentration, be it a redshift or a blueshift, appears nonuniversal, however the sum-rule results still hold.

The ongoing debate on where the holes reside in $Ga_{1-x}Mn_xAs$ has motivated many additional experiments. These include detailed IR spectroscopic studies of the IMT,[29] the dependence of the Curie temperature (T_C) on the hole concentration,[30] and resonant tunneling experiments on heterostructures,[31] all of which conclude that E_F lies within a Mn-induced IB in FM $Ga_{1-x}Mn_xAs$. In fact, the tunneling experiments found that the VB structure of GaAs is almost perfectly maintained in $Ga_{1-x}Mn_xAs$, with the exchange splitting of the VB limited to only a few meV. These conclusions are not universally accepted, however. It has been argued that the resonant tunneling results are actually due to the appearance of two-dimensional hole subbands in the GaAs:Be layer of the heterostructure, rather than due to the VB structure of the $Ga_{1-x}Mn_xAs$ layer.[32] The authors who obtained the resonant tunneling data present a rebuttal to this latter interpretation in Ref. 33. Scanning tunneling microscopy (STM) measurements find features of the local electronic structure of $Ga_{1-x}Mn_xAs$ that are difficult to reconcile with a weakly disordered VB or IB picture.[34] The STM experiments instead emphasize the prevalent role played by compensation and disorder, and the influence of electron-electron interactions near the IMT of $Ga_{1-x}Mn_xAs$.

The difficulty in obtaining a comprehensive understanding of the electronic structure of $Ga_{1-x}Mn_xAs$ is related to the high level of electronic disorder in the system. To synthesize $Ga_{1-x}Mn_xAs$, low-temperature growth protocols are required.[22] A direct but unintentional result of the low-temperature growth, and a contributing factor to disorder in the system, are high concentrations of compensating interstitial and antisite defects.[35,36] The presence of these compensating defects ensures that the carrier density p is never equal to the dopant density. However, the exact relationship between the dopant concentration and p cannot be established because of the myriad of complicated factors involved in the film growth. The uncertainty in carrier density and the effects of disorder have clouded the interpretation of experiments,[27,30,34,37] and have proven to be an imposing theoretical challenge.[20,38–40] Therefore, the systematic, disorder-free addition or removal of carriers provided by the electric field effect is highly desirable for studies of $Ga_{1-x}Mn_xAs$. Moreover, the unique access to the electronic structure and dynamics granted by our IR probe establish IR spectroscopy as an ideal experimental tool to conduct such a study.

III. EXPERIMENTAL DATA AND PROCEDURES

The films in the $Ga_{1-x}Mn_xAs$-based devices were grown using low-temperature molecular beam epitaxy (MBE) on (001) GaAs substrates. This paper reports on a $Ga_{1-x}Mn_xAs$-based device with active film grown to 100 nm, and a Mn doping density of $x = 0.015$. The Mn doping density is inferred from reflection high-energy electron diffraction intensity oscillation measurements of the MnAs growth rate.[41,42] The doping level was chosen to keep p as low as possible, yet still at a sufficient level to ensure the film is FM at low temperatures. Indeed, this (Ga,Mn)As film has a FM

transition at $T_C = 25$ K, determined by SQUID magnetometry. By limiting the carrier density in this way, the impact of the field effect on our observables is maximized. We note that our results were reproduced on a second $x = 0.015$ Ga$_{1-x}$Mn$_x$As-based device. The film of this latter device was grown to 10 nm, under the same growth protocols as the 100 nm film. This latter device is referred to as Device B, and will be relevant to the intragap spectral weight comparison made later in the paper (Sec. IV B).

The film in the Ga$_{1-x}$Be$_x$As-based device has a Be content of $x = 3.2 \times 10^{-4}$, determined by Hall-effect measurements, placing it slightly above the critical IMT concentration ($x_c = 2.7 \times 10^{-4}$) of Ga$_{1-x}$Be$_x$As.[29,43] The Be-doped film is 980 nm thick and was also grown on a (001) GaAs substrate. Ga$_{1-x}$Be$_x$As in this doping regime does not require low-temperature growth protocols. Thus the $x = 3.2 \times 10^{-4}$ Ga$_{1-x}$Be$_x$As sample was grown using conventional equilibrium MBE. We note that IR spectroscopy data for the $x = 3.2 \times 10^{-4}$ Ga$_{1-x}$Be$_x$As film were previously reported in Ref. 29 by some of the same authors as those of this work.

To quantify the effect of field-induced charges on the accumulation or depletion layer, it is imperative to extract the optical constants of the active film at $V_{gs} = 0$. These optical constants are necessary for the modeling of the transmission data of our EDL field-effect devices under applied V_{gs} discussed later. To obtain the optical constants at $V_{gs} = 0$, we first measure the room-temperature transmission spectrum of the film and GaAs substrate two-layer system, normalized by the bare substrate transmission. The transmission spectrum is then fit by a Kramers-Kronig (KK) consistent, multioscillator model. The model yields the complex conductivity spectrum of the film [$\sigma(0V,\omega) = \sigma_1(0V,\omega) + i\sigma_2(0V,\omega)$], provided the substrate optical constants are known or measured separately.[44] The real (or dissipative) part of the IR conductivity spectra, $\sigma_1(0V,\omega)$, resulting from this analysis for the (Ga,Mn)As and (Ga,Be)As films, can be seen in Figs. 2(a) and 2(b), respectively, and are discussed later in the paper.

Our EDL field-effect devices utilize an "ion gel" (a mixture of ionic liquid and block copolymer) to serve as the gate insulator. The ionic liquid used in our study is composed of 1-ethyl-3-methylimidazolium (the cation) and bis(trifluoromethylsulphonyl)imide (the anion). The block copolymer is polystyrene-poly(ethylene oxide)-polystyrene (PS-PEO-PS), and serves as a way to gel the ionic liquid for practical use in our devices. The composition of the ion gel is approximately 75% ionic liquid and 25% block copolymer. The operating principle of EDL field-effect devices is that the mobile ions of the ionic liquid move to the device interfaces upon application of V_{gs}. This forms EDLs at the interfaces [see Fig. 1(b)]. The EDLs are effectively two capacitors in series, with one across the interface of the active film and ion gel, and a second across that of the ion gel and gate electrode. We thus define $V_{eff} = \frac{A_g}{A_g + A_s} V_{gs}$, where A_s is the gated area of the active film and A_g that of the gate electrode, as the effective voltage drop across the interface of the active film and the ion gel.

Advantages of ion gels over conventional dielectrics include high charge injection density and operation at low gate voltages.[45–49] An additional advantage of ion gels specific to IR studies is that devices can be designed such that the
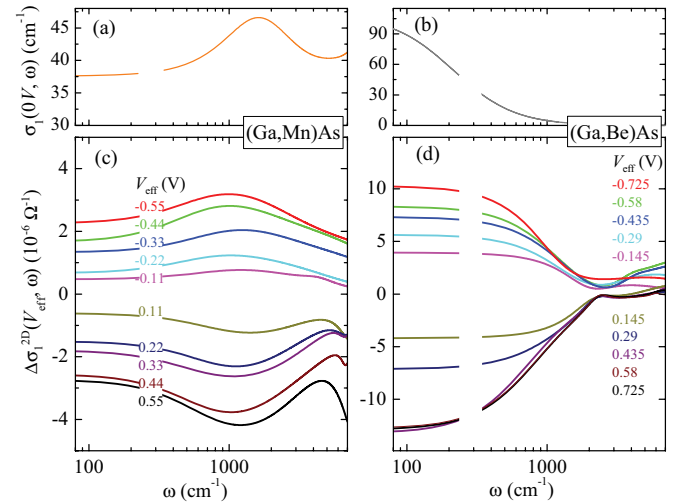

FIG. 2. (Color online) Panels (a) and (b) show the $V_{eff} = 0$ IR conductivity spectrum of the $x = 0.015$ Ga$_{1-x}$Mn$_x$As film and the $x = 3.2 \times 10^{-4}$ Ga$_{1-x}$Be$_x$As film used in our devices, respectively. The two-dimensional differential conductivity $\Delta\sigma^{2D}(V_{eff},\omega)$ spectra at all V_{eff} are shown for the (Ga,Mn)As-based device in panel (c), and for the (Ga,Be)As-based device in panel (d). The data are cut near 300 cm^{-1} due to GaAs opacity over the cut frequency range.

gate electrode is out of the optical path [see Figs. 1(a) and 1(b)]. If the gate electrode is *in* the optical path, an IR transparent conductor must be used. In this latter case, however, electrostatically induced effects in both the active film and the transparent conductor will be present in the IR spectra. We note that electrostatic effects in the transparent conductor observed in IR spectra can exceed those in the active film both in top- and back-gated devices.[50,51]

To obtain the changes to the IR conductivity spectrum induced by application of V_{eff}, transmission through the device is measured before, T($0V,\omega$), and after, T(V_{eff},ω), V_{gs} is applied. This procedure was repeated multiple times for each V_{gs}, and the transmission spectra were then averaged. The ratio T(V_{eff},ω)/T($0V,\omega$) reveals the electrostatically induced changes to the spectrum, and is plotted in Fig. 1 for both types of device. It is assumed that neither the GaAs substrate nor the active film, apart from a narrow accumulation or depletion layer at the interface of the film and ion gel, has any V_{gs} dependence to their IR response. In the case of the ion gel, electrostatically induced changes to the optical properties are confined to narrow vibrational modes, and do not show any broad effects. These assertions with regard to the ion-gel layer are confirmed by analysis of graphene-based devices.[52] We therefore attribute the changes to the spectra to the formation of a narrow accumulation or depletion layer at the interface of the active film and the ion gel.

A potential issue when dealing with EDL devices is the possibility of electrochemical reactions, which lead to permanent modification of the active material at the interface.[53] In this context, we note that such electrochemical reactions cannot repeatedly produce increased transmission in one polarity and decreased transmission in the opposite polarity, as is observed in our devices (Fig. 1). Furthermore, in our measurements, the transmission spectrum was always compared before activating,

and after turning off V_{gs}. We found that the spectra of our devices after turning off V_{gs} were always identical to the spectrum before activating V_{gs}, observing the ratio of the two spectra to be a flat line at 1.0000 ± 0.0002 over our frequency range. The "symmetric" behavior of the spectra in the two polarities, along with the absence of any effects that persist after V_{gs} is turned off, show conclusively that the results of electric field gating reported here are essentially entirely electrostatic in nature, rather than electrochemical.

To characterize the optical constants of the accumulation or depletion layer, $T(V_{eff},\omega)/T(0V,\omega)$ spectra were fit following the differential modeling protocol of the RefFIT software package.[44] The differential modeling is done in two steps. The initial step is to build a base model. In our case, the base model describes the optical constants of the film at $V_{gs} = 0$. This initial process of acquiring optical constants at $V_{gs} = 0$ was described above. The second step, after the base modeling, is to construct a differential model, which represents the change in the optical constants of the accumulation or depletion layer. This latter model is comprised of multiple oscillators whose parameters are then adjusted in order to fit the change in the measured spectrum induced by some externally controlled parameter. The fits resulting from this modeling are shown as light gray lines in Figs. 1(c) and 1(d). The differential model yields the differential conductivity spectrum, $\Delta\sigma(V_{eff},\omega) = \sigma(V_{eff},\omega) - \sigma(0V,\omega)$. This differential conductivity function satisfies the usual physical requirements of $\sigma(\omega)$, such as the KK relation.

We note that the magnitude of both $\Delta\sigma(V_{eff},\omega)$ and $\sigma(V_{eff},\omega)$ extracted from modeling are dependent on the thickness L of the accumulation or depletion layer used for the analysis. Thus, in order to model the broad changes observed in the $T(V_{eff},\omega)/T(0V,\omega)$ spectra, L must be assumed. We avoid this ambiguity by performing our analysis in two-dimensional units, and we report the two-dimensional differential conductivity spectrum, $\Delta\sigma^{2D}(V_{eff},\omega) = \Delta\sigma(V_{eff},\omega)L$. The advantage of $\Delta\sigma^{2D}(V_{eff},\omega)$ is that the L dependence is removed from the modeling, and thus $\Delta\sigma^{2D}(V_{eff},\omega)$ is independent of the actual thickness of the accumulation or depletion layer.[50,54]

IV. DISCUSSION

A. Infrared conductivity spectra

The $\Delta\sigma_1^{2D}(V_{eff},\omega)$ spectra, which represent changes to dissipative processes in the accumulation or depletion layer, of the (Ga,Be)As-based device are shown in Fig. 2(d). These data show monotonically increasing Drude-like line forms [Drude line form described by Eq. (1)] in the polarity associated with hole accumulation ($V_{eff} < 0$). In the reverse polarity ($V_{eff} > 0$), associated with hole depletion, monotonically decreasing inverted Drude-like line forms are observed for $V_{eff} = 0.0145$–0.435 V. At higher voltages, the effect appears to saturate, as the $V_{eff} = 0.58$ and 0.725 V spectra are nearly identical to that of $V_{eff} = 0.435$ V.

The $\sigma_1(0V,\omega)$ spectrum of the (Ga,Be)As film [Fig. 2(b)] is described by a prominent Drude peak, with the formula given by

$$\sigma_1(\omega) = \frac{\Gamma\sigma_{dc}}{\Gamma^2 + \omega^2}. \tag{1}$$

The Drude line form is characteristic of delocalized carriers in a metal. The amplitude at $\omega = 0$ is equal to the dc conductivity σ_{dc}, and the half width at half-maximum quantifies the scattering rate Γ. Thus, taking into account the Drude line form of the $V_{eff} = 0$ spectrum, the $\Delta\sigma_1^{2D}(V_{eff},\omega)$ spectra can be understood as enhancing or diminishing the Drude response in the accumulation and depletion polarities, respectively. The changes to the Drude response are extinguished by approximately 2500 cm^{-1} at all V_{eff}. Above 2500 cm^{-1}, much weaker changes to the spectra are observed, which are broad and featureless. As we show below in the sum-rule analysis of the (Ga,Be)As $\sigma_1(0V,\omega)$ spectrum, we conclude that E_F lies within the VB of the GaAs host. The conclusion of E_F lying within the VB for this doping is also consistent with earlier IR studies of $Ga_{1-x}Be_xAs$.[29,43] With E_F established to be in the VB, we speculate that the changes above 2500 cm^{-1} may be related to excitations from the split-off band[55] or broadening of the GaAs band-gap edge. However, these effects are not examined in detail in this work.

We note that although E_F is established as residing in the GaAs host VB of the (Ga,Be)As film, there is no feature observed in any of the (Ga,Be)As spectra consistent with transitions from the light hole (LH) to heavy hole (HH) bands. Earlier IR experiments reported in Refs. 43 and 29 have observed such a feature centered near 600–700 and 1800 cm^{-1} in $x = 8.2 \times 10^{-4}$ and $x = 0.009$ $Ga_{1-x}Be_xAs$, respectively. Based on these earlier data, any resonance due to LH $\rightarrow$ HH transitions in the film reported here should be expected to be centered below 600 cm^{-1}, and weaker than the already relatively weak feature reported for the $x = 8.2 \times 10^{-4}$ $Ga_{1-x}Be_xAs$ film of Ref. 43. Any electric field-induced modifications to such a weak feature in this latter frequency regime, if present at all, may be obscured by the absorption lines of the ion gel.

We now turn to the $\Delta\sigma_1^{2D}(V_{eff},\omega)$ spectra of the accumulation or depletion layer in the (Ga,Mn)As-based device, shown in Fig. 2(c). We first describe only the spectra in the hole accumulation polarity. In this polarity, the $\Delta\sigma_1^{2D}(V_{eff},\omega)$ spectra reveal a broad mid-IR resonance, peaked $\sim$1000 cm^{-1}, which increases monotonically in strength with voltage. Unfortunately, a more precise account of the peak frequency of the mid-IR resonance is unavailable. This limitation on the peak frequency is due to absorption modes in the ion gel, prevalent in the raw data, which obscure the spectra [see Fig 1(c)]. The $\Delta\sigma_1^{2D}(V_{eff},\omega)$ spectra also show enhancement at lower frequencies and in the limit of $\omega \rightarrow 0$. At these far-IR frequencies, the spectra are relatively flat, and show a monotonic increase in strength with voltage.

The $\sigma_1(0V,\omega)$ spectrum of the (Ga,Mn)As film [Fig. 2(a)] shows a broad mid-IR resonance peak near 2000 cm^{-1}, as well as relatively flat conductivity in the far-IR regime. These features are consistent with those reported in the literature for $Ga_{1-x}Mn_xAs$.[24,25,28,29] The far-IR contribution to the $\sigma_1(0V,\omega)$ spectrum is attributed to the electromagnetic response of itinerant carriers. Interpretation of the mid-IR resonance, however, remains a subject of debate.[25,27–29] This latter feature lies in an energy range consistent with either transitions to a Mn-induced IB, where E_F is within the IB, or intra-VB transitions from the LH to HH bands, with E_F within the VB.
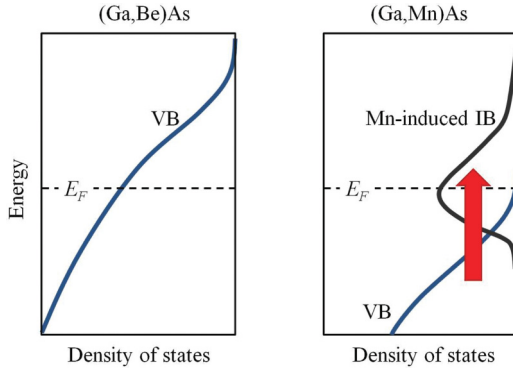
FIG. 3. (Color online) Schematic illustrating the density of states in (Ga,Be)As (left panel) and (Ga,Mn)As (right panel) according to our experimental interpretation. The red arrow in the right panel represents transitions giving rise to the mid-IR resonance in the (Ga,Mn)As data. For these interband transitions, m_{opt} is approximately equal to the VB mass, as discussed in the text.

The far-IR and mid-IR features of the $V_{eff} = 0$ spectrum for the (Ga,Mn)As film suggest a natural interpretation of the $\Delta\sigma_1^{2D}(V_{eff},\omega)$ spectra. That is, we interpret $\Delta\sigma_1^{2D}(V_{eff},\omega)$ of the (Ga,Mn)As accumulation layer as enhancing both the itinerant carrier response and the strength of the mid-IR resonance. Although it is difficult to uniquely separate out these two contributions to $\Delta\sigma_1^{2D}(V_{eff},\omega)$, we note that the $T(V_{eff},\omega)/T(0V,\omega)$ spectra cannot be reproduced without both contributions present in the model. In the depletion polarity, we observe similar features, however with the line shape "inverted." The strength of these depletion effects increases monotonically with voltage. Thus the features in the depletion polarity are interpreted as reducing the itinerant carrier response and the strength of the mid-IR resonance of the (Ga,Mn)As film.

The contrasting forms of the spectral line shapes of the (Ga,Be)As- and (Ga,Mn)As-based devices are consistent with detailed studies of the IMT in chemically doped $Ga_{1-x}Be_xAs$ and $Ga_{1-x}Mn_xAs$.[25,29,56] These latter studies show that the signatures of the Mn-induced IB are present in the spectra of FM $Ga_{1-x}Mn_xAs$ films, and that the IB plays a vital role in the electrodynamics. Thus we attribute the broad mid-IR resonance of the (Ga,Mn)As-based device spectra to VB→ IB transitions. In contrast, the spectroscopic features of the (Ga,Be)As-based device data are all indicative of metallic conduction due to extended states within the host VB. The features consistent with VB conduction in the (Ga,Be)As-based device include the sum-rule analysis reported below (Sec. IV B). A schematic representation of the density of states consistent with our data is displayed in Fig. 3.

B. Sum-rule analysis

In more common field-effect devices with oxide insulating material, the change in carrier density induced by the field effect is determined by the dielectric constant, the thickness of the oxide layer, and the applied voltage. Unfortunately in our devices, the complexities of the EDLs prevent such simple calculations of the change in hole density induced by an electric field. However, a powerful aspect of IR spectroscopy

is that it can serve as a contactless probe of the carrier density to effective mass ratio according to

$$N_{eff}(0V) = \frac{p(0V)}{m_{opt}} = \frac{2}{\pi e^2} \int_0^{\omega_c} \sigma_1(0V,\omega)d\omega, \qquad (2)$$

where N_{eff} is the "spectral weight" and ω_c is the appropriate cutoff for integration. When applied to a Drude peak alone, m_{opt} is equal to the effective band mass of the delocalized carriers.[8] In the (Ga,Be)As film, the hole density $p(0V)$ is known from room-temperature Hall effect measurements to be 7.1×10^{18} cm^{-3}. Therefore, we can extract m_{opt} of this film at $V_{eff} = 0$ by applying Eq. (2) to the $\sigma_1(0V,\omega)$ spectrum in Fig. 2(b). From this analysis, we find $m_{opt} = 0.42m_e$ for our (Ga,Be)As film at $V_{eff} = 0$, where m_e is the bare electron mass. This mass is in excellent agreement with the mass extracted from mobility data of p-type GaAs doped with nonmagnetic (Zn, C, or Be) acceptors.[57] The experimental value of m_{opt} is in accord with conduction in the GaAs host VB, where the directionally averaged density-of-state masses of the HH and LH bands are $m_{HH} = 0.5m_e$ and $m_{LH} = 0.088m_e$, respectively.[58] Applying these HH and LH band masses to the expression for the two-band transport mass, $m = (m_{HH}^{3/2} + m_{LH}^{3/2})/(m_{HH}^{1/2} + m_{LH}^{1/2})$, gives a mass of $0.38m_e$.[59]

Assuming no strong voltage dependence of m_{opt}, we can relate the two-dimensional change in hole density $\Delta p^{2D}(V_{eff}) = [p(V_{eff}) - p(0V)]L$ to the $\Delta\sigma_1^{2D}(V_{eff},\omega)$ spectra by

$$\Delta N_{eff}^{2D}(V_{eff}) = \frac{\Delta p^{2D}(V_{eff})}{m_{opt}} = \frac{2}{\pi e^2} \int_0^{\omega_c} \Delta\sigma_1^{2D}(V_{eff},\omega)d\omega. \qquad (3)$$

For the (Ga,Be)As data of Fig. 2(d), we integrate the spectra according to Eq. (3) up to $\omega_c = 2500$ cm^{-1}. This cutoff serves to isolate only the portion of $\Delta\sigma_1^{2D}(V_{eff},\omega)$ attributed to modifications of the Drude response in the (Ga,Be)As-based accumulation or depletion layer. We plot $\Delta N_{eff}^{2D}(V_{eff})$ as a function of V_{eff} in Fig. 4. As m_{opt} has been independently determined for this film as described above, the right axis of Fig. 4(b) is scaled to reveal $\Delta p^{2D}(V_{eff})$. In the hole accumulation polarity, $\Delta N_{eff}^{2D}(V_{eff})$ reveals sublinear behavior with the effect equal to 4.7×10^{12} cm^{-2}/m_e ($\Delta p^{2D} = 2.0 \times 10^{12}$ cm^{-2}) at the largest voltage, $V_{eff} = -0.725$ V. In the hole depletion polarity, $\Delta N_{eff}^{2D}(V_{eff})$ appears to saturate for $V_{eff} > 0.4$ V, as would be expected from the spectra. The largest effect in the hole depletion polarity is $\Delta N_{eff}^{2D}(V_{eff}) = -4.9 \times 10^{12}$ cm^{-2}/m_e ($\Delta p^{2D} = -2.1 \times 10^{12}$ cm^{-2}) at $V_{eff} = 0.725$ V.

In the case of the (Ga,Mn)As data, a similar "Drude-only" sum-rule analysis is complicated due to the difficulty in uniquely separating the Drude component from the mid-IR resonance in the $\Delta\sigma_1^{2D}(V_{eff},\omega)$ spectra. Detailed quantitative analysis of estimates for the "Drude mass" in $Ga_{1-x}Mn_xAs$ can be found in Refs. 24 and 25, which in general find it to be significantly larger than that of $Ga_{1-x}Be_xAs$. Additional experimental probes and theoretical studies also support large carrier masses in $Ga_{1-x}Mn_xAs$.[7,31,57,60–62]

Another useful application of the sum rule in Eq. (3) is to examine the spectra over intragap energy scales (rather than "Drude-only"). Thus, we extend the ω_c integration cutoff through the mid-IR resonance of the (Ga,Mn)As spectra while holding it sufficiently low such that contributions to the
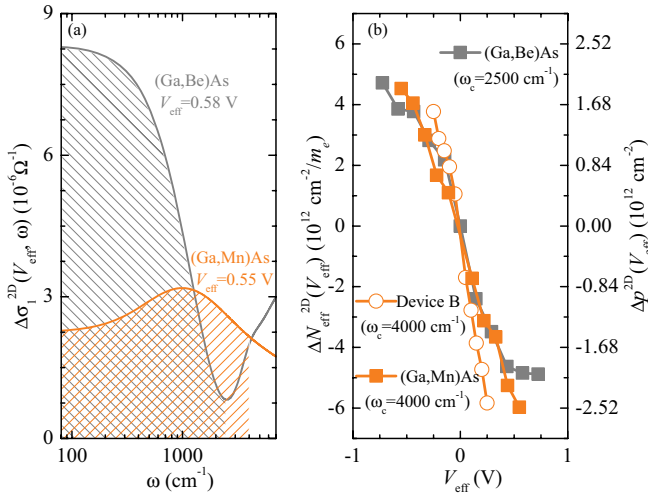
FIG. 4. (Color online) Panel (a) shows the $\Delta\sigma_1^{2D}(V_{eff},\omega)$ for the (Ga,Mn)As-based device and the (Ga,Be)As-based device at $V_{eff} =$ 0.55 and 0.58 V, respectively. The orange and gray shaded regions indicate the area included for equivalent intragap spectral weight in application of Eq. (3) for the (Ga,Mn)As and (Ga,Be)As accumulation layers, respectively. Panel (b) shows the change in spectral weight according to Eq. (3) at all V_{eff} for the (Ga,Be)As-, (Ga,Mn)As-, and second (Ga,Mn)As- (device B) based devices. The choice in integration cutoff ω_c is described in the text. Using the calibration procedure described in the text, the right axis is converted into the two-dimensional change in hole concentration, Δp^{2D}.

spectral weight from excitations into the GaAs host conduction band are excluded. In Fig. 4(a), the gray and orange shaded regions under the $\Delta\sigma_1^{2D}(V_{eff},\omega)$ spectra indicate the total area included in determining $\Delta N_{eff}^{2D}(V_{eff})$ of the $V_{eff} = 0.58$ V (Ga,Be)As ($\omega_c = 2500$ cm^{-1}) and $V_{eff} = 0.55$ V (Ga,Mn)As ($\omega_c = 3800$ cm^{-1}) accumulation layer spectra, respectively. The two shaded regions in the figure for these near-equivalent voltages mark off an identical total area. In Fig. 4(b), we generalize the intragap comparison of $\Delta N_{eff}^{2D}(V_{eff})$ of our materials. In this latter figure, we show the change in intragap spectral weight of both devices at all V_{eff}, with $\omega_c = 4000$ and 2500 cm^{-1} for the (Ga,Mn)As- and (Ga,Be)As-based devices, respectively. The data of Figs. 4(a) and 4(b) demonstrate that, in general, the $\Delta N_{eff}^{2D}(V_{eff})$ found in the (Ga,Mn)As accumulation or depletion layer is roughly equivalent to that of the (Ga,Be)As accumulation or depletion layer for a given V_{eff}.

Since the same ion gel is used in both devices, the capacitance per unit area, and thus $\Delta p^{2D}(V_{eff})$, are nominally similar in both (Ga,Mn)As- and (Ga,Be)As-based devices. We further justify this assumption by performing our IR experiments on a second $x = 0.015$ Ga$_{1-x}$Mn$_x$As-based device. We show $\Delta N_{eff}^{2D}(V_{eff})$ with $\omega_c = 4000$ cm^{-1} for this device, labeled Device B, in Fig. 4(b). We find a near-identical trend in $\Delta N_{eff}^{2D}(V_{eff})$ for Device B as in the other two devices. The agreement of this trend between the two (Ga,Mn)As-based devices in particular supports the conclusion that $\Delta p^{2D}(V_{eff})$ is behaving nominally similar in all our devices. Moreover, the corresponding $\Delta N_{eff}^{2D}(V_{eff})$ per $\Delta p^{2D}(V_{eff})$ suggests an approximate equivalence of m_{opt} as well.

We note that in the physical picture we have formulated from our data (see Fig. 3), the value of m_{opt} in the (Ga,Be)As-

and (Ga,Mn)As-based devices is due to different processes. In the (Ga,Be)As-based device, m_{opt} is extracted from intraband (Drude) excitations within the VB. In contrast, m_{opt} of the (Ga,Mn)As-based devices is a result of integrating over the broad mid-IR resonance ascribed to interband processes (and relatively weak itinerant carrier response). For interband excitations, m_{opt} is the reduced mass of the bands involved.[63] Thus when applying the sum rule over the mid-IR resonance (due to VB→ IB transitions) of the (Ga,Mn)As data, the reduced mass m_{opt} of the heavy IB and light VB will be approximately equal to the VB mass. The Drude mass of the (Ga,Be)As data is also clearly representative of the VB mass in that material. Thus according to the physical picture of Fig. 3, an identical m_{opt} of our active materials implies an equivalence of their VB masses. The fact that the Drude mass of the (Ga,Be)As film is in accord with the VB mass of GaAs supports the conclusion that Mn or Be doping does not lead to a substantial renormalization of the GaAs host VB. This latter result is in agreement with resonant tunneling spectroscopy experiments on Ga$_{1-x}$Mn$_x$As layers.[31]

V. CONCLUSION

Our results using this electrostatic or "clean" method of tuning the carrier density reveal the electrodynamics to be vastly different between the (Ga,Mn)As- and (Ga,Be)As-based devices. This difference indicates that conduction in FM Ga$_{1-x}$Mn$_x$As is distinct from genuine metallic behavior due to extended states in the host VB. The latter behavior is unmistakably exemplified by the clear enhancement or reduction of the Drude response in the accumulation or depletion layer of the (Ga,Be)As-based device. In contrast, the relatively weak effect of electrostatic doping on the far-IR conductivity, and the dominance of the broad mid-IR feature observed in the $\Delta\sigma_1(V_{eff},\omega)$ spectra of the (Ga,Mn)As-based device, highlight the unconventional nature of conduction in this FM semiconductor. Moreover, the spectroscopic features observed in this work are all consistent with the "IB picture" of FM Ga$_{1-x}$Mn$_x$As.

A growing body of experimental evidence suggests the IB plays a central role in the electrodynamics of Ga$_{1-x}$Mn$_x$As.[7,25,29,31,60,64–67] Due to the systematic nature of the addition or removal of carriers characteristic of the electric field effect, this work provides a greater level of detail on dynamical properties associated with the IB. We stress that theoretical descriptions of the electronic structure and magnetism consistent with an IB model of Ga$_{1-x}$Mn$_x$As are also in place.[11,19–21,57,61,62,68–70] This picture is in conflict, however, with the *p-d* Zener model of ferromagnetism in Ga$_{1-x}$Mn$_x$As, where the FM interaction is mediated by holes in a weakly disordered VB.[18,71] On the one hand, this latter model has successfully accounted for a number of observations related to the magnetic properties of Ga$_{1-x}$Mn$_x$As.[10,14,72,73] On the other hand, there are also numerous experimental studies of the magnetic properties in dispute with the VB *p-d* Zener model description of Ga$_{1-x}$Mn$_x$As.[30,37,74,75] Therefore, an alternative or competing FM mechanism in line with the IB picture, such as double exchange,[11,74] should be thoroughly investigated and conclusively verified. The optical detection of electrostatic modification of the accumulation layer in EDL devices established here offers a promising route for decoupling spin doping via Mn substitution and charge doping

via electric field effect. Such future studies may provide crucial information for elucidating the underlying mechanism(s) of ferromagnetism in $Ga_{1-x}Mn_xAs$.

ACKNOWLEDGMENTS

[1] C. H. Ahn, J.-M. Triscone, and J. Mannhart, Nature (London) **424**, 1015 (2003).

[2] C. H. Ahn, M. Di Ventra, J. N. Eckstein, C. D. Frisbie, M. E. Gershenson, A. M. Goldman, I. H. Inoue, J. Mannhart, A. J. Millis, A. F. Morpurgo *et al.*, Rev. Mod. Phys. **78**, 1185 (2006).

[3] K. Ueno, S. Nakamura, H. Shimotani, A. Ohtomo, N. Kimura, T. Nojima, H. Aoki, Y. Iwasa, and M. Kawasaki, Nat. Mater. **7**, 855 (2008).

[4] M. M. Qazilbash, Z. Q. Li, V. Podzorov, M. Brehm, F. Keilmann, B. G. Chae, H. T. Kim, and D. N. Basov, Appl. Phys. Lett. **92**, 241906 (2008).

[5] J. Chakhalian, A. J. Millis, and J. Rondinelli, Nat. Mater. **11**, 92 (2012).

[6] S. J. Allen, Jr., D. C. Tsui, and F. DeRosa, Phys. Rev. Lett. **35**, 1359 (1975).

[7] K. S. Burch, D. D. Awschalom, and D. N. Basov, J. Magn. Magn. Mater. **320**, 3207 (2008).

[8] D. Basov, R. Averitt, D. van der Marel, M. Dressel, and K. Haule, Rev. Mod. Phys. **83**, 471 (2011).

[9] A. H. MacDonald, P. Schiffer, and N. Samarth, Nat. Mater. **4**, 195 (2005).

[10] T. Jungwirth, J. Sinova, J. Mašek, J. Kučera, and A. H. MacDonald, Rev. Mod. Phys. **78**, 809 (2006).

[11] K. Sato, J. Kudrnovský, P. H. Dederichs, O. Eriksson, I. Turek, B. Sanyal, G. Bouzerar, H. Katayama-Yoshida, V. A. Dinh, T. Fukushima *et al.*, Rev. Mod. Phys. **82**, 1633 (2010).

[12] T. Dietl, Nat. Mater. **9**, 965 (2010).

[13] D. Chiba, F. Matsukura, and H. Ohno, Appl. Phys. Lett. **89**, 162505 (2006).

[14] M. Sawicki, D. Chiba, A. Korbecka, Y. Nishitani, J. A. Majewski, F. Matsukura, T. Dietl, and H. Ohno, Nat. Phys. **6**, 22 (2009).

[15] M. Endo, D. Chiba, H. Shimotani, F. Matsukura, Y. Iwasa, and H. Ohno, Appl. Phys. Lett. **96**, 022515 (2010).

[16] N. Samarth, Nat. Mater. **9**, 955 (2010).

[17] N. Samarth, Nat. Mater. **11**, 360 (2012).

[18] T. Dietl, H. Ohno, F. Marsukura, J. Cibert, and D. Ferrand, Science **287**, 1019 (2000).

[19] K. Sato, P. H. Dederics, and H. Katayama-Yoshida, Europhys. Lett. **61**, 403 (2003).

[20] M. Berciu and R. N. Bhatt, Phys. Rev. Lett. **87**, 107203 (2001).

[21] P. Mahadevan and A. Zunger, Appl. Phys. Lett. **85**, 2860 (2004).

[22] H. Ohno, Science **281**, 951 (1998).

[23] K. Hirakawa, S. Katsumoto, T. Hayashi, Y. Hashimoto, and Y. Iye, Phys. Rev. B **65**, 193312 (2002).

[24] E. J. Singley, R. K. Kawakami, D. D. Awschalom, and D. N. Basov, Phys. Rev. Lett. **89**, 097203 (2002).

[25] K. S. Burch, D. B. Shrekenhamer, E. J. Singley, J. Stephens, B. L. Sheu, R. K. Kawakami, P. Schiffer, N. Samarth, D. D. Awschalom, and D. N. Basov, Phys. Rev. Lett. **97**, 087208 (2006).

[26] J. Sinova, T. Jungwirth, S.-R. Yang, J. Kučera, and A. H. MacDonald, Phys. Rev. B **66**, 041202 (2002).

[27] T. Jungwirth, J. Sinova, A. H. MacDonald, B. L. Gallagher, V. Novák, K. W. Edmonds, A. W. Rushforth, R. P. Campion, C. T. Foxon, L. Eaves *et al.*, Phys. Rev. B **76**, 125206 (2007).

[28] T. Jungwirth, P. Horodyská, N. Tesarová, P. Němec, J. Šubrt, P. Malý, P. Kužel, C. Kadlec, J. Mašek, I. Němec *et al.*, Phys. Rev. Lett. **105**, 227201 (2010).

[29] B. C. Chapler, R. C. Myers, S. Mack, A. Frenzel, B. C. Pursley, K. S. Burch, E. J. Singley, A. M. Dattelbaum, N. Samarth, D. D. Awschalom *et al.*, Phys. Rev. B **84**, 081203 (2011).

[30] M. Dobrowolska, K. Tivakornsasithorn, X. Liu, J. K. Furdyna, M. Berciu, K. M. Yu, and W. Walukiewicz, Nat. Mater. **11**, 444 (2012).

[31] S. Ohya, K. Takata, and M. Tanaka, Nat. Phys. **7**, 342 (2011).

[32] T. Dietl and D. Sztenkiel, arXiv:1102.3267.

[33] S. Ohya, K. Takata, I. Muneta, P. N. Hai, and M. Tanaka, arXiv:1102.4459.

[34] A. Richardella, P. Roushan, S. Mack, B. Zhou, D. A. Huse, D. D. Awschalom, and A. Yazdani, Science **327**, 665 (2010).

[35] K. Edmonds, P. Boguslawski, K. Wang, R. Campion, S. Novikov, N. Farley, B. Gallagher, C. Foxon, M. Sawicki, T. Dietl *et al.*, Phys. Rev. Lett. **92**, 037201 (2004).

[36] M. Missous, J. Appl. Phys. **75**, 3396 (1994).

[37] L. Rokhinson, Y. Lyanda-Geller, Z. Ge, S. Shen, X. Liu, M. Dobrowolska, and J. Furdyna, Phys. Rev. B **76**, 161201 (2007).

[38] S.-R. Yang and A. H. MacDonald, Phys. Rev. B **67**, 155202 (2003).

[39] C. P. Moca, B. Sheu, N. Samarth, P. Schiffer, B. Janko, and G. Zarand, Phys. Rev. Lett. **102**, 137203 (2009).

[40] F. Kyrychenko and C. Ullrich, Phys. Rev. B **83**, 205206 (2011).

[41] F. Schippan, Appl. Phys. Lett. **76**, 834 (2000).

[42] R. C. Myers, B. L. Sheu, A. W. Jackson, A. C. Gossard, P. Schiffer, N. Samarth, and D. D. Awschalom, Phys. Rev. B **74**, 155203 (2006).

[43] Y. Nagai and K. Nagasaka, Infr. Phys. Technol. **48**, 1 (2006).

[44] A. Kuzmenko, *Guide to Reffit: Software to Fit Optical Spectra* (2004), http://optics.unige.ch/alexey/reffit.html.

[45] C. Lu, Q. Fu, S. Huang, and J. Liu, Nano Lett. **4**, 623 (2004).

[46] H. Shimotani, H. Asanuma, A. Tsukazaki, A. Ohtomo, M. Kawasaki, and Y. Iwasa, Appl. Phys. Lett. **91**, 082106 (2007).

[47] A. Dhoot, C. Israel, X. Moya, N. Mathur, and R. Friend, Phys. Rev. Lett. **102**, 136402 (2009).

[48] A. Das, S. Pisana, B. Chakraborty, S. Piscanec, S. K. Saha, U. V. Waghmare, K. S. Novoselov, H. R. Krishnamurthy, A. K. Geim, A. C. Ferrari *et al.*, Nat. Nanotechnol. **3**, 210 (2008).

[49] R. Scherwitzl, P. Zubko, C. Lichtensteiger, and J.-M. Triscone, Appl. Phys. Lett. **95**, 222114 (2009).

[50] Z. Q. Li, V. Podzorov, N. Sai, M. C. Martin, M. E. Gershenson, M. Di Ventra, and D. N. Basov, Phys. Rev. Lett. **99**, 016403 (2007).

[51]N. Sai, Z. Li, M. Martin, D. Basov, and M. Di Ventra, Phys. Rev. B **75**, 045307 (2007).

[52]L. Ju, B. Geng, J. Horng, C. Girit, M. Martin, Z. Hao, H. A. Bechtel, X. Liang, A. Zettl, Y. R. Shen *et al.*, Nat. Nanotech. **6**, 630 (2011).

[53]K. Ueno, H. Shimotani, Y. Iwasa, and M. Kawasaki, Appl. Phys. Lett. **96**, 252107 (2010).

[54]D. C. Tsui, S. J. Allen, Jr., R. A. Logan, A. Kamgar, and S. N. Coppersmith, Surf. Sci. **73**, 419 (1978).

[55]R. Braunstein and E. O. Kane, J. Phys. Chem. Solids **23**, 1423 (1962).

[56]E. J. Singley, K. S. Burch, R. K. Kawakami, J. Stephens, D. D. Awschalom, and D. N. Basov, Phys. Rev. B **68**, 165204 (2003).

[57]K. Alberi, K. Yu, P. Stone, O. Dubon, W. Walukiewicz, T. Wojtowicz, X. Liu, and J. Furdyna, Phys. Rev. B **78**, 075201 (2008).

[58]J. Blakemore, J. Appl. Phys. **53**, 123 (1982).

[59]J. Wiley and M. DiDomenico, Jr., Phys. Rev. B **2**, 427 (1970).

[60]M. A. Mayer, P. R. Stone, N. Miller, H. M. Smith, O. D. Dubon, E. E. Haller, K. M. Yu, W. Walukiewicz, X. Liu, and J. K. Furdyna, Phys. Rev. B **81**, 045205 (2010).

[61]G. Bouzerar and R. Bouzerar, New J. Phys. **13**, 023002 (2011).

[62]C. P. Moca, G. Zaránd, and M. Berciu, Phys. Rev. B **80**, 165202 (2009).

[63]M. Dressel and G. Grüner, *Electrodynamics of Solids* (Cambridge University Press, Cambridge, MA, 2002).

[64]J. Okabayashi, A. Kimura, O. Rader, T. Mizokawa, A. Fujimori, T. Hayashi, and M. Tanaka, Phys. Rev. B **64**, 125304 (2001).

[65]E. Kojima, J. Héroux, R. Shimano, Y. Hashimoto, S. Katsumoto, Y. Iye, and M. Kuwata-Gonokami, Phys. Rev. B **76**, 195323 (2007).

[66]K. Ando, H. Saito, K. C. Agarwal, M. C. Debnath, and V. Zayets, Phys. Rev. Lett. **100**, 067204 (2008).

[67]S. Ohya, I. Muneta, P. N. Hai, and M. Tanaka, Phys. Rev. Lett. **104**, 167204 (2010).

[68]R. Bouzerar and G. Bouzerar, Europhys. Lett. **92**, 47006 (2010).

[69]M. Berciu, R. Chakarvorty, Y. Y. Zhou, M. T. Alam, K. Traudt, R. Jakiela, A. Barcz, T. Wojtowicz, X. Liu, J. K. Furdyna *et al.*, Phys. Rev. Lett. **102**, 247202 (2009).

[70]J.-M. Tang and M. Flatté, Phys. Rev. Lett. **101**, 157203 (2008).

[71]T. Jungwirth, K. Wang, and K. Edmonds, Phys. Rev. B **72**, 165204 (2005).

[72]M. Sawicki, J. Magn. Magn. Mater. **300**, 1 (2006).

[73]Y. Nishitani, D. Chiba, M. Endo, M. Sawicki, F. Matsukura, T. Dietl, and H. Ohno, Phys. Rev. B **81**, 045208 (2010).

[74]B. L. Sheu, R. C. Myers, J.-M. Tang, N. Samarth, D. D. Awschalom, P. Schiffer, and M. E. Flatte, Phys. Rev. Lett. **99**, 227205 (2007).

[75]S. Mack, R. C. Myers, J. T. Heron, A. C. Gossard, and D. D. Awschalom, Appl. Phys. Lett. **92**, 192502 (2008).